

# Supporting Information

## Anomalously Rapid Tunneling: Charge Transport across SAMs of Oligoethylene Glycol

*Mostafa Baghbanzadeh,<sup>a†</sup> Carleen M. Bowers,<sup>a†</sup> Dmitrij Rappoport,<sup>a</sup> Tomasz Łaba,<sup>b</sup> Li Yuan,<sup>a</sup> Kyungtae Kang,<sup>a</sup> Kung-Ching Liao,<sup>a</sup> Mathieu Gonidec,<sup>a</sup> Philipp Rothmund,<sup>a</sup> Piotr Cyganik,<sup>b</sup> Alan Aspuru-Guzik,<sup>a</sup> and George M. Whitesides<sup>a,c,d,\*</sup>*

<sup>a</sup>Department of Chemistry and Chemical Biology, Harvard University,  
12 Oxford Street, Cambridge, Massachusetts 02138 United States

<sup>b</sup>Smoluchowski Institute of Physics, Jagiellonian University, Lojasiewicza 11, 30-348 Krakow,  
Poland

<sup>c</sup>Kavli Institute for Bionano Science & Technology, Harvard University,  
29 Oxford Street, Massachusetts 02138 United States

<sup>d</sup>Wyss Institute of Biologically Inspired Engineering, Harvard University  
60 Oxford St. Cambridge, MA 02138, USA

\*Corresponding author, email: [gwhitesides@gmwgroup.harvard.edu](mailto:gwhitesides@gmwgroup.harvard.edu)

<sup>†</sup>Both authors contributed equally to this work.

## Table of Content

1.	Experimental Details	3
1.1.	Materials	3
1.2.	Formation of SAMs of Oligo(ethylene glycol)s on Au	3
1.3.	Characterization of SAMs of Oligo(ethylene glycol)s on Au	3
1.3.1.	Estimation of Thickness for SAMs of Oligo(ethylene glycol)s on Au using Fixed-Angle XPS	3
1.3.2.	Estimation of Thickness for SAMs of Oligo(ethylene glycol)s on Au using Angle Resolved XPS	5
1.3.4.	Estimation of Thickness for SAMs of OEGn on Au using Ellipsometry	9
1.3.5.	Influence of Incubation Time on Thickness Values for SAMs of Oligo(ethylene glycol)s	9
1.3.6.	IRRAS Analysis on SAMs of Oligo(ethylene glycol)s on Au	10
1.3.7.	Static Contact Angles with Water	12
1.4.	Electrical Measurements using Ga <sub>2</sub> O <sub>3</sub> /EGaIn Top-Electrodes	13
1.5.	Influence of the Substrate and Anchoring Group on the Electrical Measurements across SAMs of oligo(ethylene glycol)s	16
1.6.	Computational Details	19
1.6.1.	General Information	19
1.6.2.	Superexchange Model for DFT-Derived Tunneling Parameters	24
2.	Supporting Text	27
2.1.	Summary of Previous Results on Tunneling Conductivity using EGaIn as the Top Electrode	27
2.2.	SAMs Bearing Terminal Groups of Ethylene Glycol for Applications in Protein Resistance	27
	References	28

## 1. Experimental Details

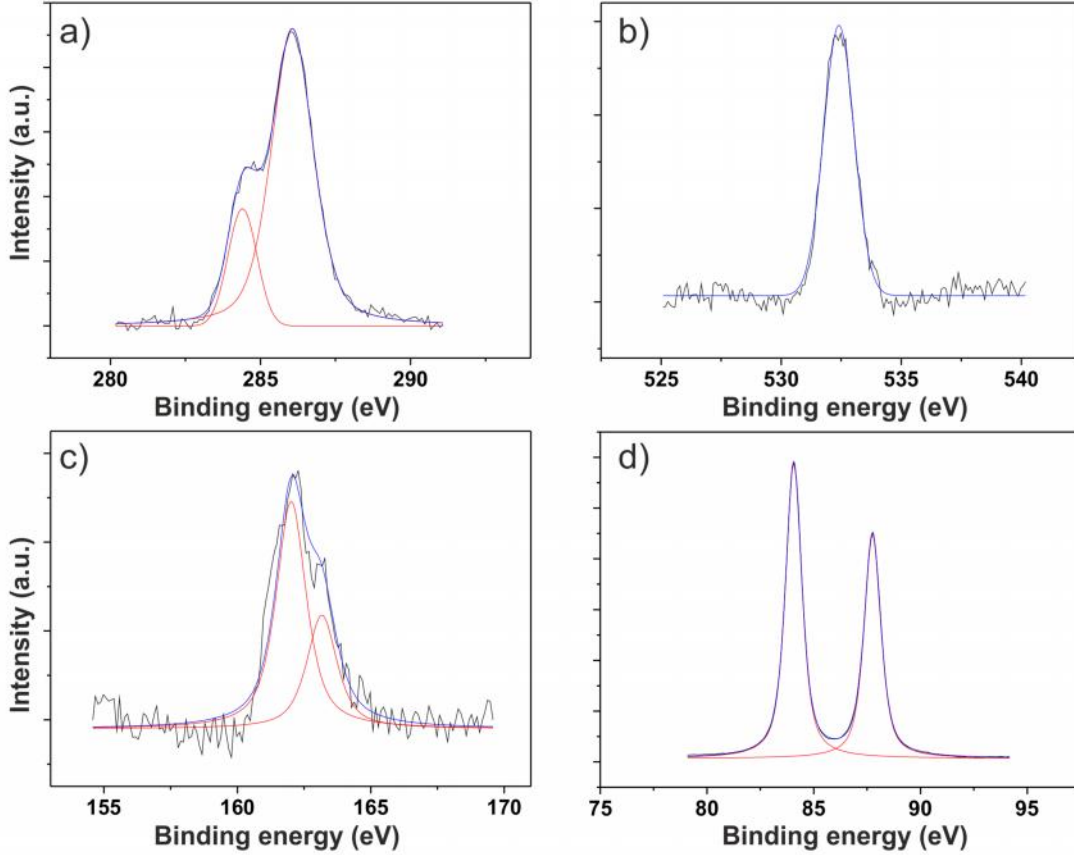
**1.1. Materials.** Molecular precursors to all self-assembled monolayers (SAMs) were commercially available (>98%, Sigma-Aldrich and BroadPharm). All organic solvents were analytical grade (99%, Sigma-Aldrich) and were used as supplied. All thiols were stored under a nitrogen atmosphere; the *n*-alkanethiols were stored at 4°C and the thiol-terminated oligo(ethylene glycol)s were stored at -20°C to avoid degradation. To ensure that the compounds were free of contaminants, all stored compounds were checked by <sup>1</sup>H NMR prior to use.

**1.2. Formation of SAMs of Oligo(ethylene glycol)s on Au.** Studies conducted by Meuse and coworkers on SAMs of thiol terminated oligoethylene glycol (HS(CH<sub>2</sub>CH<sub>2</sub>O)<sub>6</sub>CH<sub>3</sub>) concluded that solvent affects the quality of the SAMs. Their measurements on SAMs of HS(CH<sub>2</sub>CH<sub>2</sub>O)<sub>6</sub>CH<sub>3</sub> on gold indicate that ethanol results in well-ordered helical conformations on gold substrate, whereas THF leads to disorder in the films<sup>1</sup>. Following the method of Meuse and coworkers, we formed SAMs on template-stripped gold (Au<sup>TS</sup>) substrates<sup>2</sup> using solutions of thiol (~3mM) dissolved in anhydrous ethanol. The ethanolic solutions were purged with nitrogen before introduction of the metal substrate. The metal substrates were submerged in a 3 mM ethanolic solution of thiol for 24 hours at room temperature and under an atmosphere of nitrogen. We rinsed the SAM-bound substrates with ethanol, and dried them under a gentle stream of nitrogen.

### 1.3. Characterization of SAMs of Oligo(ethylene glycol)s on Au

**1.3.1. Estimation of Thickness for SAMs of Oligo(ethylene glycol)s on Au using Fixed-Angle XPS.** We estimated the thickness for SAMs of oligo(ethylene glycol)s (HS(CH<sub>2</sub>CH<sub>2</sub>O)<sub>n</sub>CH<sub>3</sub>) using fixed-angle X-ray Photoelectron Spectroscopy (XPS). The XPS data was acquired using a Thermo Scientific K-Alpha photoelectron spectrometer with Al K $\alpha$  X-ray source equipped with the monochromator and operated at the base pressure  $\sim 10^{-9}$  Torr. Figure S1 summarizes the XPS signals for C1s, O1s, S2p and Au4f on a SAM of HS(CH<sub>2</sub>CH<sub>2</sub>O)<sub>4</sub>CH<sub>3</sub>. The C1s signal (Figure S1a) has two peaks present at 284.4 eV and 286 eV, which correspond to C-C and C-O bonds. The O1s signal (Figure S1b) has a single peak present at 532.4 eV, which

corresponds to O-C bonds. The S2p signal (Figure S1c) has a doublet peak present at 162 and 163.2 eV, which confirms the formation of a S-Au bond.



**Figure S1.** XPS spectra for SAMs of HS(CH<sub>2</sub>CH<sub>2</sub>O)<sub>4</sub>CH<sub>3</sub> on Au. (a) C1s signal with peaks at 284.4 eV and 286 eV. (b) O1s signal with a peak at 532.4 eV. (c) S2p signal with a doublet at 162 eV and 163.2 eV. (d) Au4f signal with a doublet peak at 84 eV and 87.7 eV.

To estimate the thickness of the SAMs of HS(CH<sub>2</sub>CH<sub>2</sub>O)<sub>4</sub>CH<sub>3</sub> on Au, we calculated the ratio of the C1s signal intensity to the Au4f signal intensity according to eq. S1,

$$\frac{\alpha I_{C1s}}{I_{Au4f}} = K \frac{1 - e^{-\frac{d-d_c}{\lambda_C}}}{e^{-\frac{d}{\lambda_{Au}}}} \quad (S2)$$

where  $I_{C1s}$ ,  $I_{Au4f}$  are the intensities of the C1s and Au4f signals. The  $\alpha \approx 3/2$  parameter considers the reduced C1s signal compared to that obtained for *n*-alkanes, which are used here as a reference SAM. The inelastic mean free path parameter ( $\lambda$ ) for the C1s and Au4f signals is  $\lambda_C$

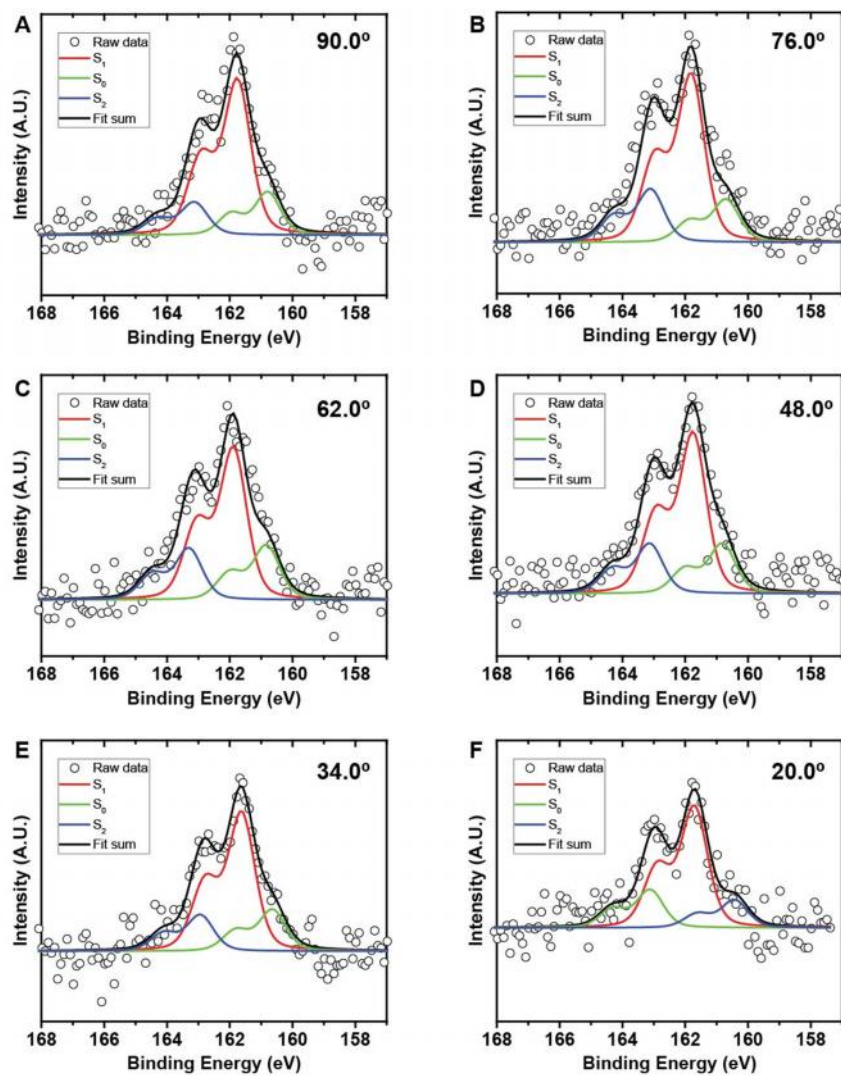
= 3.15 nm and  $\lambda_{Au} = 3.45$  nm. These values are based on data reported by Lamont and Wilkes.<sup>3</sup> The Parameter  $d_C = 0.28$  nm indicates the distance between the first C atom of the HS(CH<sub>2</sub>CH<sub>2</sub>O)<sub>n</sub>CH<sub>3</sub> chain and the Au surface to which it is bound. We determined the value of the apparatus parameter  $K$  by measuring a SAM of tetradecanethiol on Au(111), and also by using values of film thickness for alkanethiols reported previously by Grunze and coworkers.<sup>4</sup> Table S1 summarizes our results for the measured thicknesses of HS(CH<sub>2</sub>CH<sub>2</sub>O)CH<sub>3</sub>, and compares them to calculated values of length, assuming both all-trans and helical conformations.

**Table S1.** Comparison of calculated lengths and experimental thicknesses for SAMs of HS(CH<sub>2</sub>CH<sub>2</sub>O)<sub>n</sub>CH<sub>3</sub>. The lengths were calculated assuming an all-trans extended conformation and a helical conformation. The lengths were calculated using DFT with B3LYP and def2-SVP functional, resolution-of-the-identity approximation (RI-J). The experimental thicknesses were calculated using fixed-angle XPS analysis.

HS(CH <sub>2</sub> CH <sub>2</sub> O) <sub>n</sub> CH <sub>3</sub>	Calculated Length (Å)		Experimental Thickness using Fixed-Angle XPS (Å)
	All-Trans Conformation	Helical Conformation	
HS(CH <sub>2</sub> CH <sub>2</sub> O) <sub>2</sub> CH <sub>3</sub>	9.5	8.8	6.5
HS(CH <sub>2</sub> CH <sub>2</sub> O) <sub>3</sub> CH <sub>3</sub>	13.1	10.5	11.7
HS(CH <sub>2</sub> CH <sub>2</sub> O) <sub>4</sub> CH <sub>3</sub>	16.6	13.3	10.5
HS(CH <sub>2</sub> CH <sub>2</sub> O) <sub>5</sub> CH <sub>3</sub>	20.1	16.2	12.3
HS(CH <sub>2</sub> CH <sub>2</sub> O) <sub>6</sub> CH <sub>3</sub>	23.7	19.0	11.8
HS(CH <sub>2</sub> CH <sub>2</sub> O) <sub>7</sub> CH <sub>3</sub>	27.2	21.4	12.7

**1.3.2. Estimation of Thickness for SAMs of Oligo(ethylene glycol)s on Au using Angle Resolved XPS.** In addition to estimating film thicknesses of oligo(ethylene glycol)s using fixed-angle XPS, we also measured the thickness values for SAMs of HS(CH<sub>2</sub>CH<sub>2</sub>O)<sub>n</sub>CH<sub>3</sub> (n = 2-7) on Au<sup>TS</sup> using angle-resolved XPS. The emission angle (indicated in Figure S2) is defined as the angle between the axis of the analyzer and the substrate surface. The difference between the angle of the incident X-ray and the emission angle is fixed at 50°. The angle-resolved XPS spectra are taken by rotating the sample stage to the desired emission angles. All S2p spectra were corrected with a Shirley background and fitted to Voigt functions (constant ratio of 30% to 70% for Lorentzian to Gaussian). Figure S2 shows an example of the S2p spectra collected for a SAM of HS(CH<sub>2</sub>CH<sub>2</sub>O)<sub>5</sub>CH<sub>3</sub> on Au<sup>TS</sup>. Using previously reported peak assignments,<sup>5-7</sup> we assigned the following peak fits: i) S<sub>1</sub> (~161.8 eV), which corresponds to the chemically

adsorbed components, ii)  $S_2$  (~163 eV), which corresponds to the physical adsorbed components, and iii)  $S_0$  (~160.8 eV), which corresponds to adsorption at defect sites (e.g. step-edges, grain boundaries, etc.).



**Figure S2.** High resolution XPS spectra for the S 2p peak obtained at six different angles of analysis for a SAM of  $\text{HS}(\text{CH}_2\text{CH}_2\text{O})_5\text{CH}_3$  on  $\text{Au}^{\text{TS}}$ .

To normalize the area of irradiation of the incident X-ray using different incident angles ( $\chi$ ), we calculated the effective intensity ( $I_{\text{eff}}$ ) using eq S2:

$$I_{\text{eff}} = I \cos (90^\circ - \chi) \quad (\text{S2})$$

As indicated in eq S1, the effective intensity of the S 2p spectra decays exponentially over a distance described eq S3:<sup>8-9</sup>

$$I_\theta = I_0 \exp (-d_{\text{S-Vac}} / (\lambda \sin \theta)) \quad (\text{S3})$$

where  $\lambda$  is the inelastic mean free path,  $\lambda = 30.08 \text{ \AA}$  when the kinetic energy of the photoelectrons are  $\sim 1320 \text{ eV}$ ,<sup>3</sup>  $I_0$  is the initial intensity from S atom,  $d_{\text{S-Vac}}$  is the distance from S atoms to vacuum (e.g., the top of the SAM).

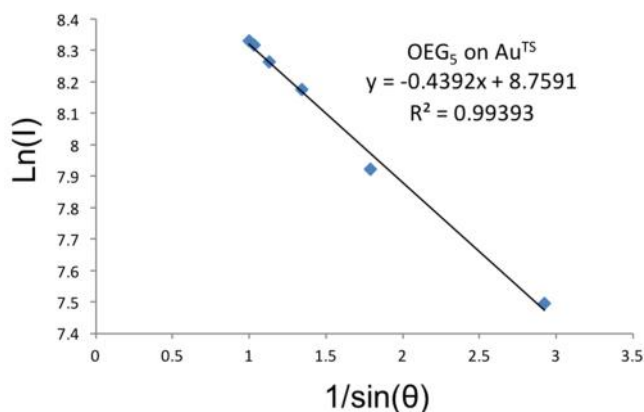
We calculated the thicknesses,  $d$ , for SAMs of  $\text{HS}(\text{CH}_2\text{CH}_2\text{O})_n\text{CH}_3$  on  $\text{Au}^{\text{TS}}$  using the sum of theoretical distance of the metal-sulfur bond ( $d_{\text{S-Au}} = 2.45 \text{ \AA}$ )<sup>10</sup> and  $d_{\text{S-Vac}}$ , as shown in eq. S4.

$$d = d_{\text{S-Vac}} + d_{\text{S-Au}} \quad (\text{S4})$$

We used the intensity of S to calculate the value of  $d$  by fitting eq. 4 (derived from eq. S3) to a plot of  $\ln(I_{\text{S}})$  vs.  $1/\sin \theta$ .

$$\ln(I_{\text{eff}}) = \ln(I_{0,\text{S}}) - d_{\text{S-Vac}} / (\lambda \sin \theta) \quad (\text{S5})$$

Figure S3 shows an example of the calculation for a SAM of  $\text{HS}(\text{CH}_2\text{CH}_2\text{O})_5\text{CH}_3$  on  $\text{Au}^{\text{TS}}$  where the slope is  $d_{\text{S-Vac}} / \lambda$ .



**Figure S3.** Plot of  $\ln(I_{eff})$  as a function of  $1/\sin\theta$  for the SAMs of  $\text{HS}(\text{CH}_2\text{CH}_2\text{O})_5\text{CH}_3$  ( $\text{OEG}_5$ ) on  $\text{Au}^{\text{TS}}$ .

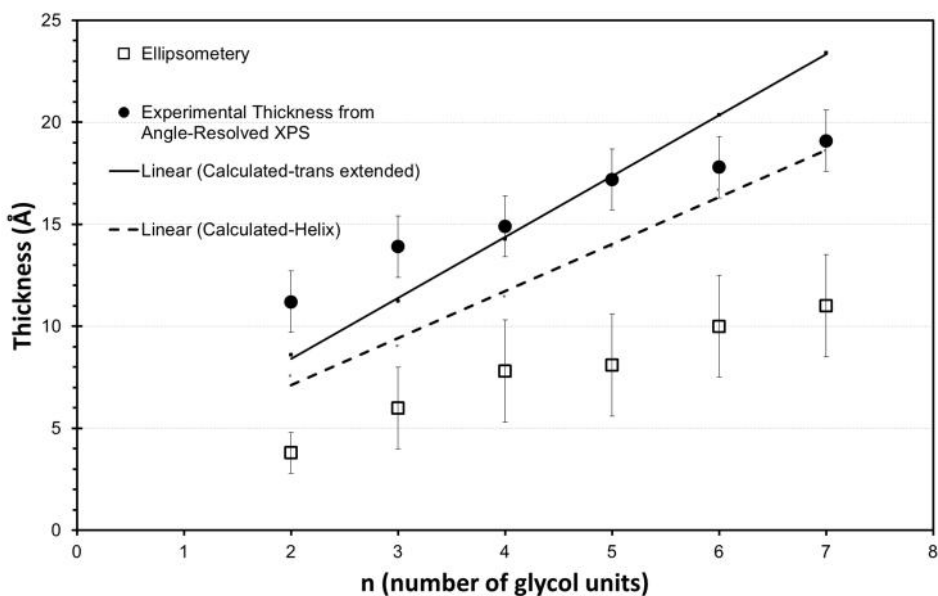
The results of thicknesses for SAMs of  $\text{HS}(\text{CH}_2\text{CH}_2\text{O})_n\text{CH}_3$  ( $n = 2-7$ ) on  $\text{Au}^{\text{TS}}$  using angle-resolved XPS and fixed-angle XPS analysis are summarized in Table S2. The error bars, estimated from the Gaussian fits to the S 2p spectra, are  $\sim 1.5 \text{ \AA}$ .

**Table S2.** Comparison of experimental thicknesses for SAMs of  $\text{HS}(\text{CH}_2\text{CH}_2\text{O})_n\text{CH}_3$  using fixed-angle XPS and angle-resolved XPS.

$\text{HS}(\text{CH}_2\text{CH}_2\text{O})_n\text{CH}_3$	Experimental Thickness using Fixed-Angle XPS ( $\text{\AA}$ )	Experimental Thickness using Angle-Resolved XPS ( $\text{\AA}$ )
$\text{HS}(\text{CH}_2\text{CH}_2\text{O})_2\text{CH}_3$	6.5	$11.2 \pm 1.5$
$\text{HS}(\text{CH}_2\text{CH}_2\text{O})_3\text{CH}_3$	11.7	$13.9 \pm 1.5$
$\text{HS}(\text{CH}_2\text{CH}_2\text{O})_4\text{CH}_3$	10.5	$14.9 \pm 1.5$
$\text{HS}(\text{CH}_2\text{CH}_2\text{O})_5\text{CH}_3$	12.3	$17.2 \pm 1.5$
$\text{HS}(\text{CH}_2\text{CH}_2\text{O})_6\text{CH}_3$	11.8	$17.8 \pm 1.5$
$\text{HS}(\text{CH}_2\text{CH}_2\text{O})_7\text{CH}_3$	12.7	$19.8 \pm 1.5$

Figure S4 compares the experimental thicknesses (measured by angle-resolved XPS) with calculated lengths for both all-trans and helical conformations. The thickness values of  $\text{HS}(\text{CH}_2\text{CH}_2\text{O})_n\text{CH}_3$  are comparable with the all-trans lengths when  $n = 2$  and  $3$ . When  $n > 3$ , the thicknesses are comparable with the lengths of the helical conformations.





**Figure S4.** Plot of calculated lengths and experimental thickness values for  $\text{HS}(\text{CH}_2\text{CH}_2\text{O})_n\text{CH}_3$ . The lengths for all-trans and helical conformations were calculating using DFT with B3LYP and def2-SVP functional, resolution-of-the-identity approximation (RI-J). The experimental thicknesses were calculated using angle-resolved XPS and single-wavelength scanning ellipsometry.

#### 1.3.4. Estimation of Thickness for SAMs of Oligo(ethylene glycol)s on Au using

**Ellipsometry.** We also measured the thickness for SAMs of  $\text{HS}(\text{CH}_2\text{CH}_2\text{O})_n\text{CH}_3$  on  $\text{Au}^{\text{TS}}$  using ellipsometry. The data were obtained at a constant incidence angle of  $70^\circ$  using a single-wavelength scanning ellipsometer (LSE-W model, Gaertner Scientific). The spectroscopic results were simulated using the LGEMP software provided by the manufacturer using an index of refraction between of 1.46 and 1.48. To compensate for the possible heterogeneity in composition across the surface, measurements were taken at ten different positions on at least two different surfaces.

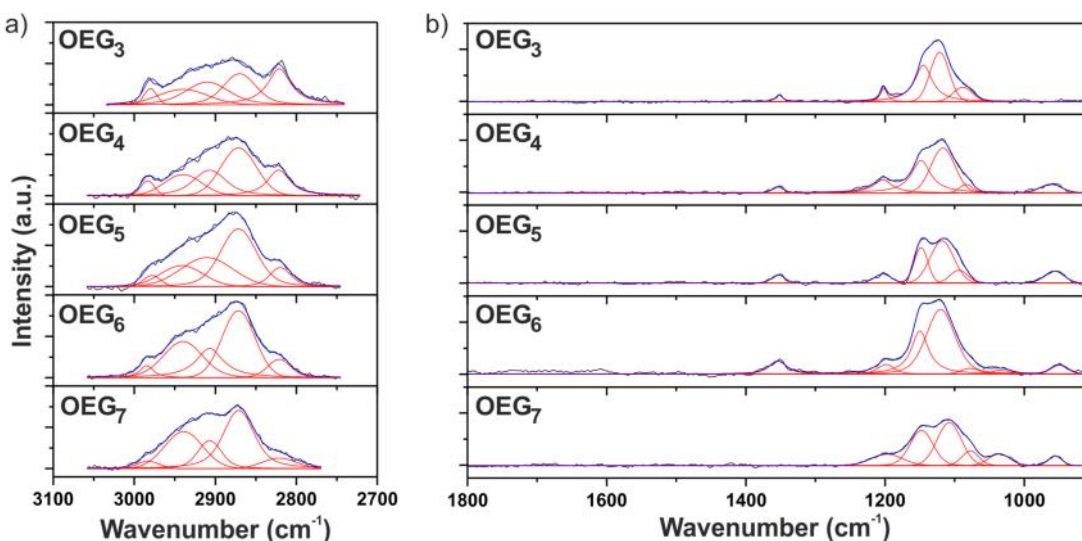
#### 1.3.5. Influence of Incubation Time on Thickness Values for SAMs of Oligo(ethylene glycol)s.

We also investigated the influence of incubation time on the thicknesses of the SAMs; that is, we measured thickness using angle-resolved XPS after allowing the SAMs to form for i) 16-24 hours and ii) 1 week. This comparison is summarized in Table S3. Despite the large difference in incubation time, the resulting values of thickness do not differ by more than  $1.5 \text{ \AA}$ .

**Table S3.** Influence of incubation time during SAM formation on the measured thickness ( $\text{\AA}$ ) values using angle-resolved XPS. SAMs were incubated for 16-24 hours and 1 week.

HS(CH <sub>2</sub> CH <sub>2</sub> O) <sub>n</sub> CH <sub>3</sub>	Thickness ( $\text{\AA}$ )	Thickness ( $\text{\AA}$ )
	Incubation time = 16-24 hours	Incubation time = 1 week
HS(CH <sub>2</sub> CH <sub>2</sub> O) <sub>2</sub> CH <sub>3</sub>	11.2	11.3
HS(CH <sub>2</sub> CH <sub>2</sub> O) <sub>3</sub> CH <sub>3</sub>	13.9	13.6
HS(CH <sub>2</sub> CH <sub>2</sub> O) <sub>4</sub> CH <sub>3</sub>	14.9	17
HS(CH <sub>2</sub> CH <sub>2</sub> O) <sub>5</sub> CH <sub>3</sub>	17.2	16
HS(CH <sub>2</sub> CH <sub>2</sub> O) <sub>6</sub> CH <sub>3</sub>	17.8	17.2
HS(CH <sub>2</sub> CH <sub>2</sub> O) <sub>7</sub> CH <sub>3</sub>	19.8	19.1

**1.3.6. IRRAS Analysis on SAMs of Oligo(ethylene glycol)s on Au.** To further characterize the SAMs of HS(CH<sub>2</sub>CH<sub>2</sub>O)<sub>n</sub>CH<sub>3</sub> we investigated the structural conformation of the molecules using IR Reflection Absorption Spectroscopy (IRRAS). Figure S5 summarizes the IRRAS data obtained for a SAMs of HS(CH<sub>2</sub>CH<sub>2</sub>O)<sub>n</sub>CH<sub>3</sub>.



**Figure S5.** IRRAS spectra for SAMs of HS(CH<sub>2</sub>CH<sub>2</sub>O)<sub>n</sub>CH<sub>3</sub> (OEG; n = 3-7) on Au in the C-H (a) and C-O or C-C (b) region. See Table S4 for a detailed description of each sub-band. The range of presented spectra was chosen to match the data reported by Meuse and coworkers.<sup>11</sup>

We analyzed the IRRAS data in two wavenumber regions: 3100-2700 cm<sup>-1</sup> and 1800-900 cm<sup>-1</sup> and fitted the spectra with Voigt-shaped peaks to identify the characteristic vibrations bands (Table S4). We identified the formation of multiple conformational phases (helical, all-trans, and

amorphous) in the monolayer for all lengths of HS(CH<sub>2</sub>CH<sub>2</sub>O)<sub>n</sub>CH<sub>3</sub> (n = 3-7). The identification of multiple conformational structures by IRRAS is compatible with the XPS data for film thickness, and suggests the formation of a higher molecular footprint for molecules of oligo(ethylene glycol)s on the surface of Au compared to molecules that adopt an all-trans extended conformation (*i.e.*, alkanethiols). That is, the high molecular footprint of oligo(ethylene glycol)s on the surface may contribute to the difference between the experimental film thickness (measured by both fixed-angle and angle-resolved XPS) and the calculated lengths (assuming an all-trans extended conformation).

We extended the 1800-900 cm<sup>-1</sup> range to enable a direct comparison to the IRRAS spectra reported by Meuse and coworkers for i) well-ordered SAMs of HS(CH<sub>2</sub>CH<sub>2</sub>O)<sub>5</sub>CH<sub>3</sub> and HS(CH<sub>2</sub>CH<sub>2</sub>O)<sub>6</sub>CH<sub>3</sub> and ii) disordered SAMs of HS(CH<sub>2</sub>CH<sub>2</sub>O)<sub>3</sub>CH<sub>3</sub> and HS(CH<sub>2</sub>CH<sub>2</sub>O)<sub>4</sub>CH<sub>3</sub>.<sup>11</sup> Despite following their procedure for SAM formation, we did not observe the highly-crystalline phases that they observe for SAMs of HS(CH<sub>2</sub>CH<sub>2</sub>O)<sub>5</sub>CH<sub>3</sub> and HS(CH<sub>2</sub>CH<sub>2</sub>O)<sub>6</sub>CH<sub>3</sub>.

**Table S4.** IR mode assignments for SAMs of HS(CH<sub>2</sub>CH<sub>2</sub>O)<sub>n</sub>CH<sub>3</sub> on Au(111) using ref. <sup>12</sup> and <sup>13</sup>.

Peaks position [cm <sup>-1</sup> ]	Mode assignment
2984	CH <sub>3</sub> asym stretch
2939	EG CH <sub>3</sub> sym stretch
2906	EG CH <sub>2</sub> sym stretch
2871	EG CH <sub>2</sub> sym stretch
2821	CH <sub>3</sub> sym stretch
1354	CH <sub>2</sub> wag
1198	EG CH <sub>2</sub> twist
1149	C-O, C-C stretch
1120	C-O, C-C stretch
1077	C-O, C-C stretch
1034	C-O, C-C stretch
949	CH <sub>2</sub> rock gauche, C-C stretch

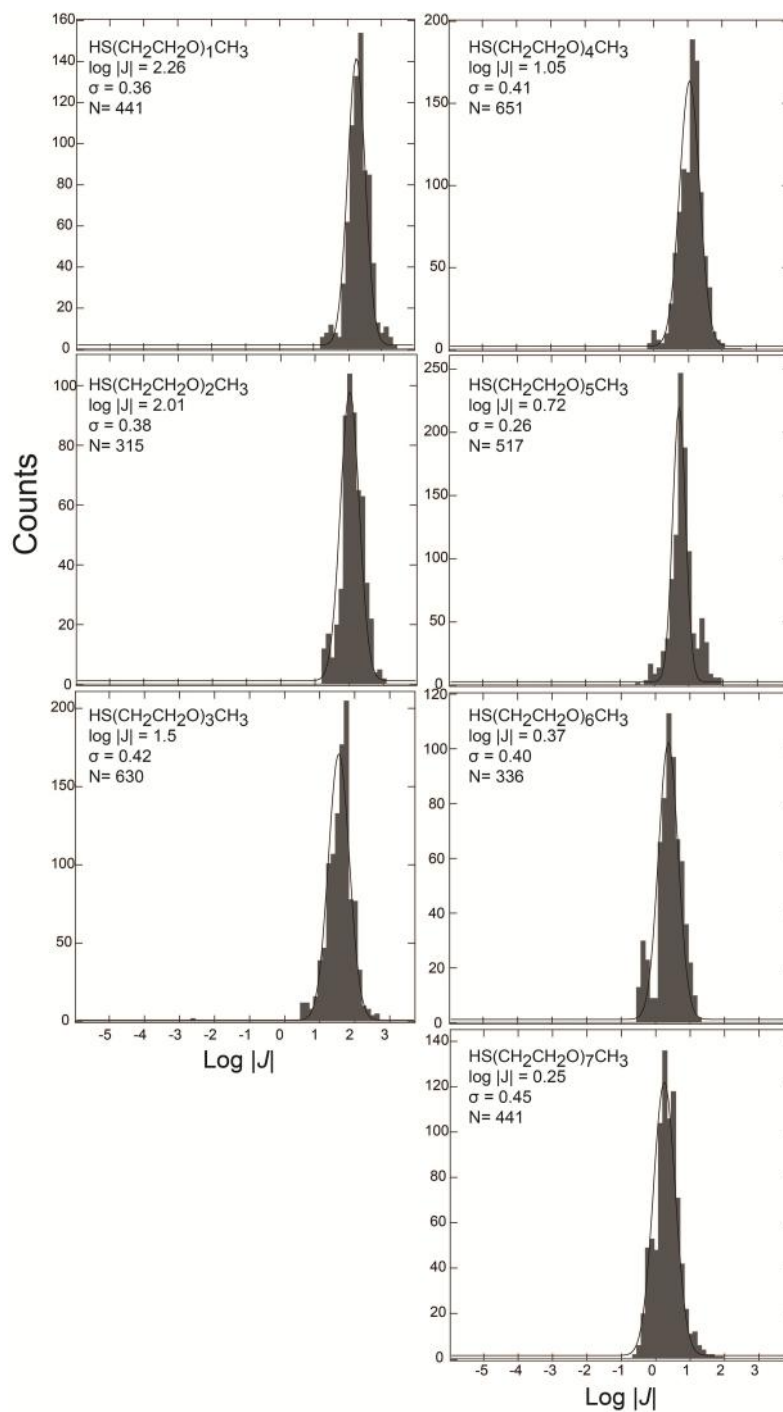
**1.3.7. Static Contact Angles with Water.** Table S5 summarizes the static contact angles with water for SAMs of HS(CH<sub>2</sub>CH<sub>2</sub>O)<sub>n</sub>CH<sub>3</sub> (n = 1-7). The values range from 37°-50°, which are lower than that reported for well-ordered SAMs of HS(CH<sub>2</sub>CH<sub>2</sub>O)<sub>6</sub>CH<sub>3</sub> (70°).<sup>1</sup> These results suggest that perhaps the terminal -OCH<sub>3</sub> group of the SAM is not oriented perpendicular to the surface. This hypothesis is compatible with the increased molecular footprint concluded from the XPS, and also with the multiple structural conformations (all-trans, helical, and amorphous) identified by IRRAS analysis.

**Table S5.** Summary of static water-wetting contact angles (°) for SAMs of HS(CH<sub>2</sub>CH<sub>2</sub>O)<sub>n</sub>CH<sub>3</sub> on Au<sup>TS</sup>

SAM on Au <sup>TS</sup>	Mean static contact angle (°) and standard deviation
HS(CH <sub>2</sub> CH <sub>2</sub> O) <sub>1</sub> CH <sub>3</sub>	49 ± 1
HS(CH <sub>2</sub> CH <sub>2</sub> O) <sub>2</sub> CH <sub>3</sub>	48 ± 2
HS(CH <sub>2</sub> CH <sub>2</sub> O) <sub>3</sub> CH <sub>3</sub>	50 ± 2
HS(CH <sub>2</sub> CH <sub>2</sub> O) <sub>4</sub> CH <sub>3</sub>	48 ± 2
HS(CH <sub>2</sub> CH <sub>2</sub> O) <sub>5</sub> CH <sub>3</sub>	38 ± 3
HS(CH <sub>2</sub> CH <sub>2</sub> O) <sub>6</sub> CH <sub>3</sub>	38 ± 1
HS(CH <sub>2</sub> CH <sub>2</sub> O) <sub>7</sub> CH <sub>3</sub>	37 ± 2

**1.4. Electrical Measurements using Ga<sub>2</sub>O<sub>3</sub>/EGaIn Top-Electrodes.** We used EGaIn (eutectic Ga-In; 74.5% Ga, 25.5% In) conical tip electrodes that were selected to be free of visible asperities on the surface of the Ga<sub>2</sub>O<sub>3</sub>; that is, so-called “selected tips”.<sup>14</sup> We measured charge-transport across the SAMs on Au<sup>TS</sup> at ±0.5 V by sweeping in both directions starting at 0 V (*i.e.*, one sweep 0 V → +0.5 V → 0 V → 0.5 V → 0 V, in steps of 0.05 V). Data for current density  $J$  (A/cm<sup>2</sup>) across SAMs of aromatic molecules exhibited a log-normal distribution; we fit Gaussian curves to histograms. We estimated the values of  $\beta$  (Å<sup>-1</sup>) and  $J_0$  (A/cm<sup>2</sup>) from the simplified Simmons equation using linear regression analyses of the variation of values of  $\langle \log|J| \rangle$  (Gaussian mean value of data for  $\log|J|$ ) with the length  $d$  (Å) of the molecule (measured as the distance in Å between the anchoring atom, S, and the distal H-atom of the molecules).

The value of  $\beta$  from the simplified Simmons equation is lower for SAMs of oligoethylene glycol than for SAMs of alkanethiolates; the decrease in  $\beta$  coincides with a decrease in  $J_0$ . (We also observed this trend for electrical measurements across SAMs of oligophenyls<sup>15</sup> and across SAMs of oligopeptides<sup>16</sup>). The interpretation of the differences in the value of  $J_0$  across these various SAMs is not (at present) straightforward, although the correlation of low values of  $\beta$  with decreased values of  $J_0$  seems to hold over a number of series.<sup>17-20</sup>

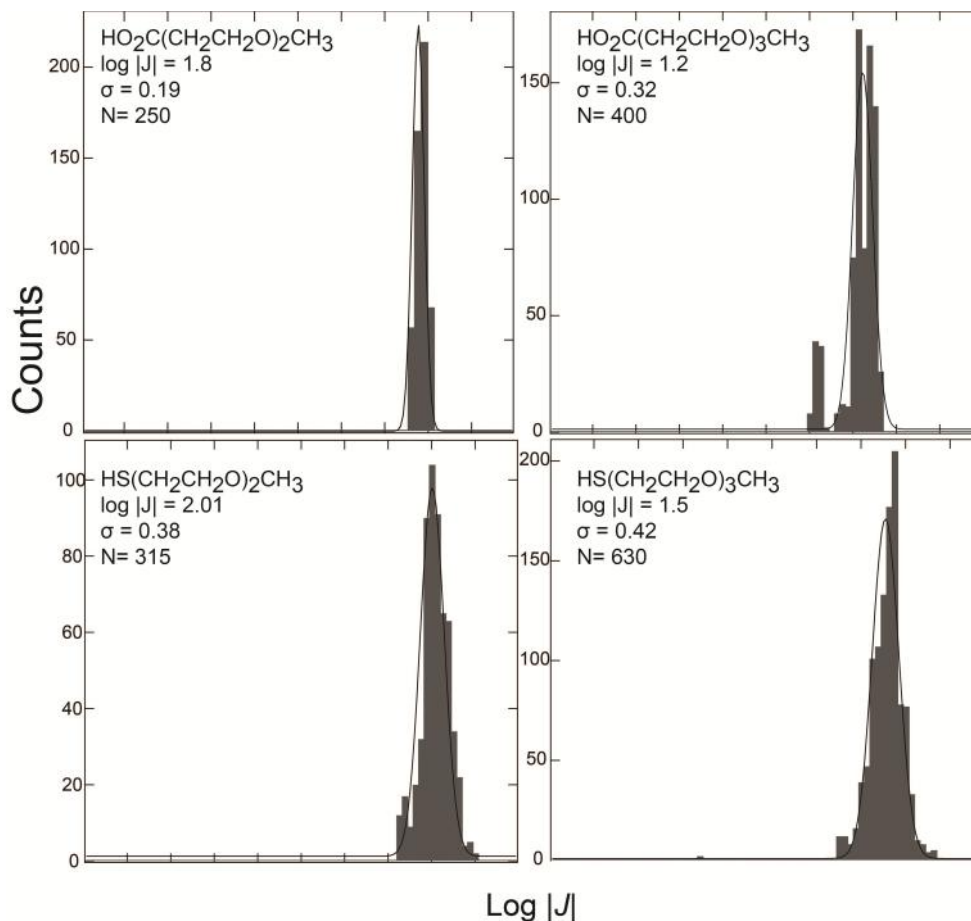


**Figure S6.** Histograms of  $\log|J|$  at +0.5 V for across SAMs of oligo(ethylene glycol)s on Au<sup>TS</sup> using selected conical tips that were free of visible surface asperities.<sup>3</sup> Solid curves indicate a Gaussian fit and  $N$  indicates the number of data points.

**Table S6.** Summary of the results for measurements of electrical tunneling across SAMs of oligo(ethylene glycol)s on Au<sup>TS</sup>. V = +0.5 V.

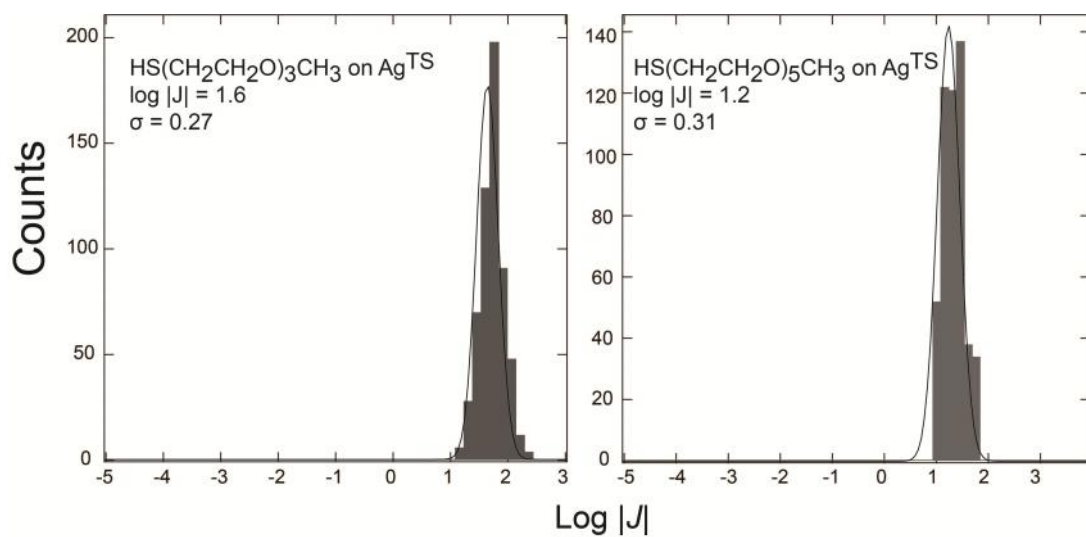
SAM	Number of Junctions	Traces	$\langle \log  J  \rangle$ V=+0.5 V	$\dagger_{\log}$	1
HS(CH <sub>2</sub> CH <sub>2</sub> O) <sub>1</sub> CH <sub>3</sub>	21	441	2.3	0.4	
HS(CH <sub>2</sub> CH <sub>2</sub> O) <sub>2</sub> CH <sub>3</sub>	15	315	2.0	0.4	
HS(CH <sub>2</sub> CH <sub>2</sub> O) <sub>3</sub> CH <sub>3</sub>	30	630	1.5	0.4	
HS(CH <sub>2</sub> CH <sub>2</sub> O) <sub>4</sub> CH <sub>3</sub>	31	651	1.0	0.4	
HS(CH <sub>2</sub> CH <sub>2</sub> O) <sub>5</sub> CH <sub>3</sub>	28	517	0.7	0.3	
HS(CH <sub>2</sub> CH <sub>2</sub> O) <sub>6</sub> CH <sub>3</sub>	16	336	0.4	0.4	
HS(CH <sub>2</sub> CH <sub>2</sub> O) <sub>7</sub> CH <sub>3</sub>	21	441	0.2	0.4	
				<b>Log  J<sub>0</sub> </b>	2.9 ± 0.1
					0.24 ± 0.01 Å <sup>-1</sup>
S(CH <sub>2</sub> ) <sub>n</sub> CH <sub>3</sub>				<b>Log  J<sub>0</sub> </b>	4.2 ± 0.1
					0.77 ± 0.02 Å <sup>-1</sup>

**1.5. Influence of the Substrate and Anchoring Group on the Electrical Measurements across SAMs of oligo(ethylene glycol)s.** To determine the influence of the bottom interface on the tunneling behavior, we measured the current density for i) thiol-bound oligo(ethylene glycol)s on Au<sup>TS</sup> and ii) carboxylate-bound oligo(ethylene glycol)s on Ag<sup>TS</sup> (Figure S7). The current densities are similar between the two classes of molecules on silver and gold for comparable lengths of ethylene glycol.

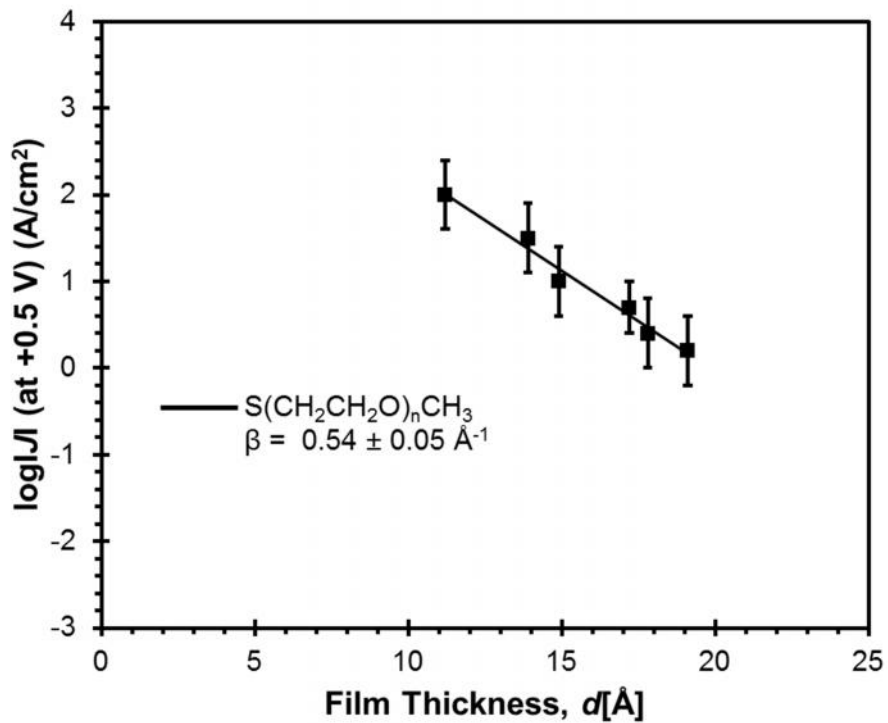


**Figure S7.** Current density measurements for SAMs of HO<sub>2</sub>C(CH<sub>2</sub>CH<sub>2</sub>O)<sub>n</sub>CH<sub>3</sub> on Ag<sup>TS</sup> (top) and for SAMs of HS(CH<sub>2</sub>CH<sub>2</sub>O)<sub>n</sub>CH<sub>3</sub> on Au<sup>TS</sup> (bottom).





**Figure S8.** Current density measurements for SAMs of HS(CH<sub>2</sub>CH<sub>2</sub>O)<sub>n</sub>CH<sub>3</sub> (n = 3 and 5) on Ag<sup>TS</sup>.

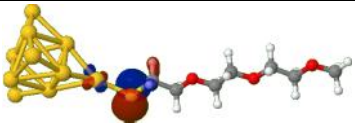
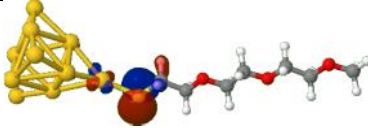
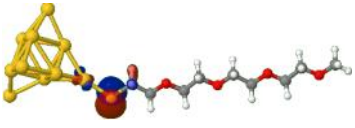
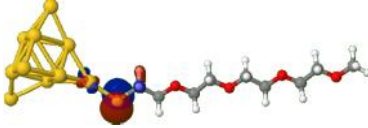
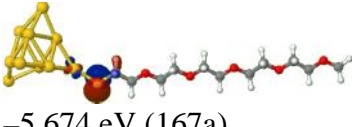
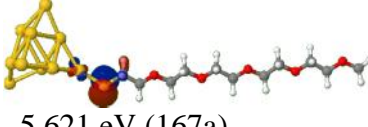
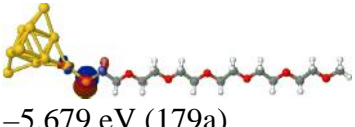
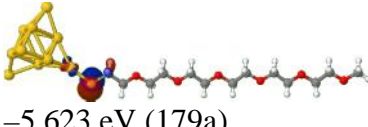
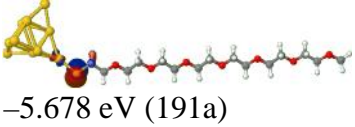
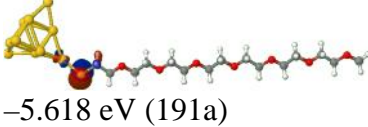
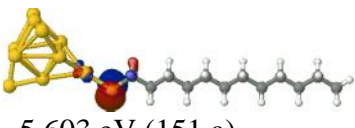
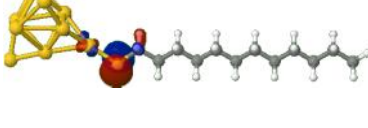


**Figure S9.** Plot of the Gaussian mean values of  $\log|J|$  at +0.5 V *versus* the film thickness for SAMs of oligo(ethylene glycol)s on Au<sup>TS</sup>. The thickness values were measured experimentally using angle-resolved XPS. The error bars represent the standard deviation of the Gaussian mean values.

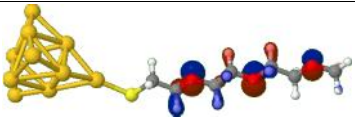
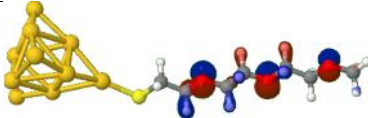
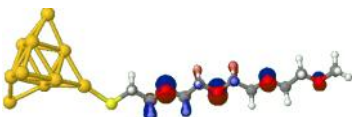
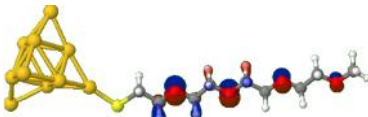
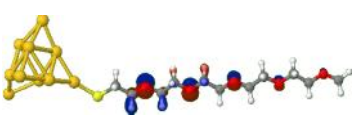
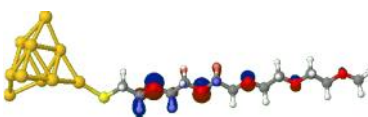
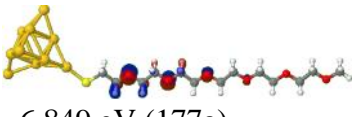
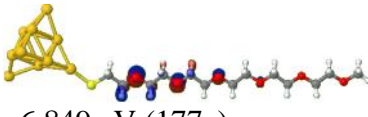
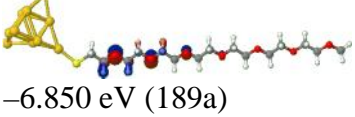
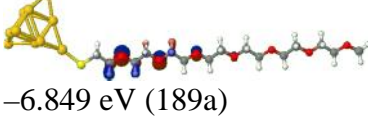
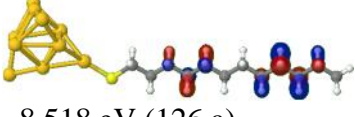
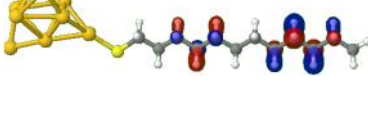
## 1.6. Computational Details.

**1.6.1. General Information.** We performed density functional theory (DFT) calculations on cluster models of gold-bound compounds of thiol-terminated oligoethylene glycols and *n*-alkanethiolates using the B3LYP hybrid exchange-correlation functional<sup>21</sup> and the resolution-of-the-identity approximation for the Coulomb interaction.<sup>22</sup> We employed split-valence plus polarization basis sets,<sup>23</sup> along with the corresponding auxiliary basis sets,<sup>24</sup> and small-core relativistic effective core potentials for Au<sup>25</sup> throughout. We carried out unrestricted structure optimizations on individual molecules attached to the Au<sub>10</sub> metal clusters. We analyzed subsequently the orbital energies and orbital shapes of the molecular orbitals (MOs) of the metal–molecule complexes at their respective optimized structures. All computations used the Turbomole quantum chemical program suite.<sup>26</sup> Spin-up (alpha) and spin-down (beta) MOs are shown separately. The results are tabulated in Tables S7 and S8.



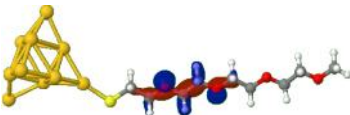

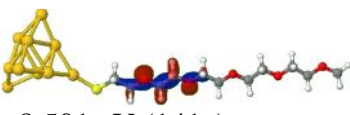
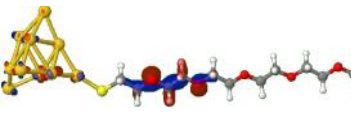
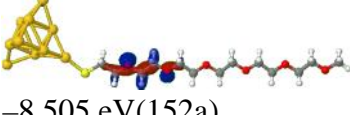
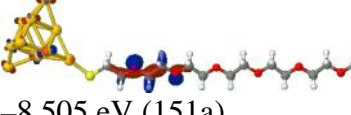
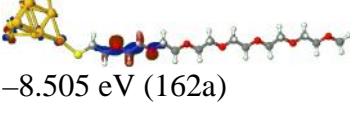
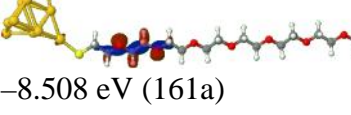


**Table S7.** Orbital energies (eV) for the molecular orbitals (MO) localized on the sulfur atom for the thiol-terminated oligoethylene glycol series and dodecanthiolate on Au<sub>10</sub> clusters. The oligomer chains assume all-trans conformations. Spin-up (alpha) and spin-down (beta) MOs are shown separately

Cluster	MO, S alpha	MO, S beta
Au <sub>10</sub> S(CH <sub>2</sub> CH <sub>2</sub> O) <sub>3</sub> CH <sub>3</sub>	 -5.672 eV (143a)	 -5.617 eV (143a)
Au <sub>10</sub> S(CH <sub>2</sub> CH <sub>2</sub> O) <sub>4</sub> CH <sub>3</sub>	 -5.678 eV (155a)	 -5.621 eV (155a)
Au <sub>10</sub> S(CH <sub>2</sub> CH <sub>2</sub> O) <sub>5</sub> CH <sub>3</sub>	 -5.674 eV (167a)	 -5.621 eV (167a)
Au <sub>10</sub> S(CH <sub>2</sub> CH <sub>2</sub> O) <sub>6</sub> CH <sub>3</sub>	 -5.679 eV (179a)	 -5.623 eV (179a)
Au <sub>10</sub> S(CH <sub>2</sub> CH <sub>2</sub> O) <sub>7</sub> CH <sub>3</sub>	 -5.678 eV (191a)	 -5.618 eV (191a)
Au <sub>10</sub> S(CH <sub>2</sub> ) <sub>11</sub> CH <sub>3</sub>	 -5.603 eV (151 a)	 -5.544 eV (151a)

**Table S8.** Orbital energies (eV) for the molecular orbitals (MO) localized on the lone pair of oxygen and the C-H bond for the thiol-terminated oligoethylene glycol series and the corresponding values for the MOs on the C-H bond of dodecanethiolate. The oligomer chains assume all-trans conformations. Spin-up (alpha) and spin-down (beta) MOs are shown separately.

Cluster	MO, O/C-H alpha	MO, O/C-H beta
$\text{Au}_{10}\text{S}(\text{CH}_2\text{CH}_2\text{O})_3\text{CH}_3$	 -6.817 eV (141a)	 -6.817 eV (141a)
$\text{Au}_{10}\text{S}(\text{CH}_2\text{CH}_2\text{O})_4\text{CH}_3$	 -6.833 eV (153a)	 -6.833 eV (153a)
$\text{Au}_{10}\text{S}(\text{CH}_2\text{CH}_2\text{O})_5\text{CH}_3$	 -6.843 eV (165a)	 -6.842 eV (165a)
$\text{Au}_{10}\text{S}(\text{CH}_2\text{CH}_2\text{O})_6\text{CH}_3$	 -6.849 eV (177a)	 -6.849 eV (177a)
$\text{Au}_{10}\text{S}(\text{CH}_2\text{CH}_2\text{O})_7\text{CH}_3$	 -6.850 eV (189a)	 -6.849 eV (189a)
$\text{SAu}_{10}\text{S}(\text{CH}_2)_{11}\text{CH}_3$	 -8.518 eV (126 a)	 -8.518 eV (126 a)

**Table S9.** Orbital energies (eV) for the molecular orbitals (MO) localized on C-C bond for the thiol-terminated oligoethylene glycol series and dodecanthiolate on Au<sub>10</sub> clusters. The oligomer chains assume all-trans conformations. Spin-up (alpha) and spin-down (beta) MOs are shown separately.

Cluster	MO, C-C alpha	MO, C-C beta
Au <sub>10</sub> S(CH <sub>2</sub> CH <sub>2</sub> O) <sub>3</sub> CH <sub>3</sub>	 -8.475 eV (120a)	 -8.475 eV (119a)
Au <sub>10</sub> S(CH <sub>2</sub> CH <sub>2</sub> O) <sub>4</sub> CH <sub>3</sub>	 -8.495 eV (130a)	 -8.495 eV (129a)
Au <sub>10</sub> S(CH <sub>2</sub> CH <sub>2</sub> O) <sub>5</sub> CH <sub>3</sub>	 -8.501 eV (141a)	 -8.501 eV (140a)
Au <sub>10</sub> S(CH <sub>2</sub> CH <sub>2</sub> O) <sub>6</sub> CH <sub>3</sub>	 -8.505 eV (152a)	 -8.505 eV (151a)
Au <sub>10</sub> S(CH <sub>2</sub> CH <sub>2</sub> O) <sub>7</sub> CH <sub>3</sub>	 -8.505 eV (162a)	 -8.508 eV (161a)
Au <sub>10</sub> S(CH <sub>2</sub> ) <sub>11</sub> CH <sub>3</sub>	 -8.078 eV (138a)	 -8.045 eV (138 a)

**Table S10.** HOMO energies, vertical ionization potentials (VIP), and HOMO–LUMO gaps of HS(CH<sub>2</sub>CH<sub>2</sub>O)<sub>n</sub>CH<sub>3</sub> (n = 3–7) in vacuum. The computational approach is identical to that used for the molecule–metal complexes.

HS(EG) <sub>n</sub> OCH <sub>3</sub>	<i>E</i> (HOMO), eV	VIP, eV	<i>E</i> (gap), eV
n = 3	−6.313	8.264	7.036
n = 4	−6.318		7.036
n = 5	−6.320		7.036
n = 6	−6.322		7.036
n = 7	−6.323		7.036

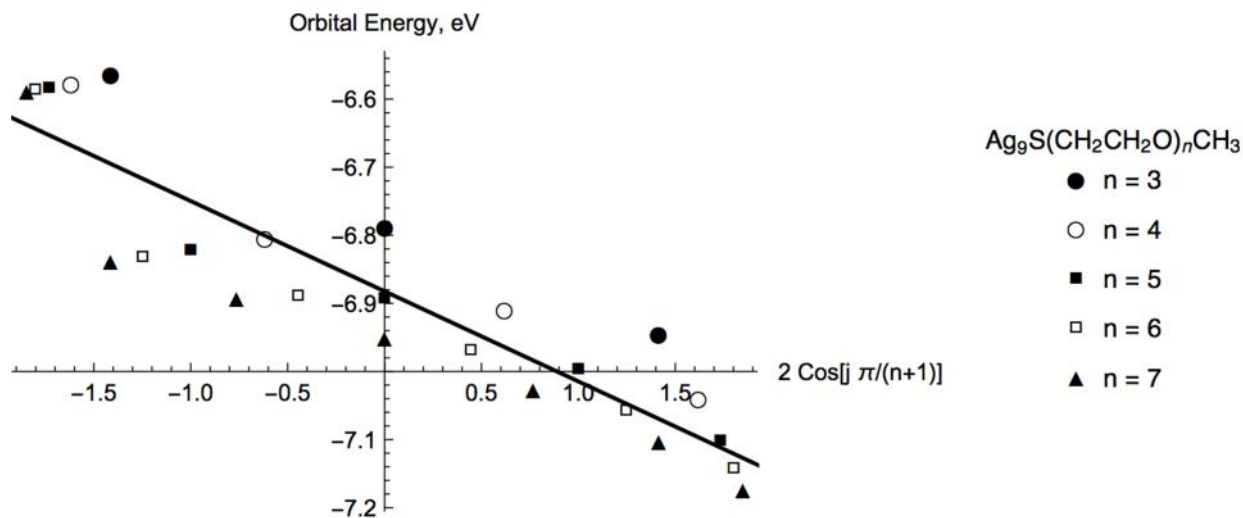
**Table S11.** HOMO energies, vertical ionization potentials (VIP), and HOMO–LUMO gaps of HS(CH<sub>2</sub>)<sub>n</sub>CH<sub>3</sub> (n = 9–17) in vacuum. The computational approach is identical to that used for the molecule–metal complexes.

HS(CH <sub>2</sub> ) <sub>n</sub> CH <sub>3</sub>	<i>E</i> (HOMO), eV	VIP, eV	<i>E</i> (gap), eV
n = 9	−6.181	8.585	7.057
n = 11	−6.181	8.492	7.057
n = 13	−6.181	8.413	7.057
n = 15	−6.180	8.346	7.057
n = 17	−6.180	8.289	7.057

**1.6.2. Superexchange Model for DFT-Derived Tunneling Parameters.** The superexchange model considers  $n$  localized oxygen lone-pair orbitals of energy  $e_0$  interacting with each other via nearest-neighbor coupling  $V$ . As a result of the orbital interaction, the orbital energies of the  $n$  localized oxygen lone-pair orbitals are split according to the following expression, which is analogous to linear polyenes  $C_nH_{n+2}$ <sup>10</sup>,

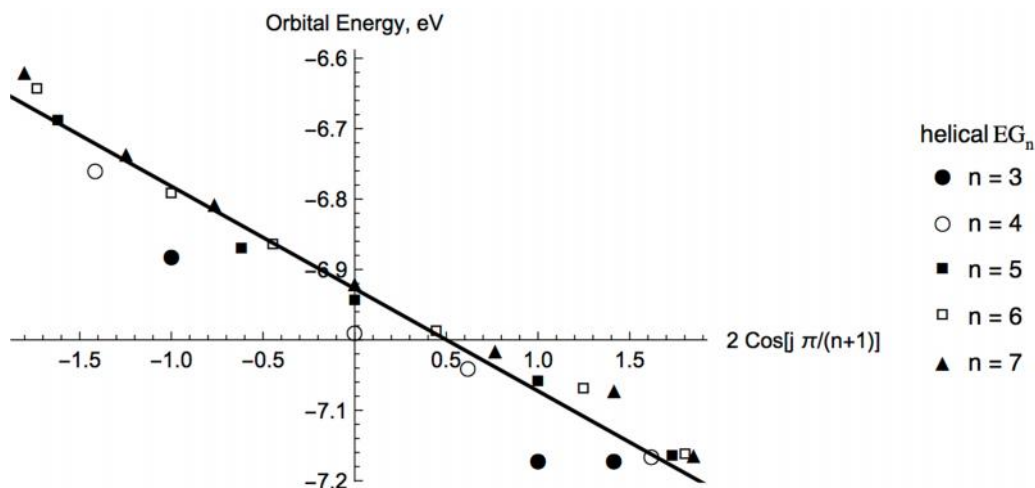
$$e_j = e_0 + 2V \cos\left(\frac{j\pi}{n+1}\right), \quad j = 1, \dots, n,$$

The parameters  $e_0$  and  $V$  can thus be obtained by linear regression of orbital energies computed using DFT. The regression results for the thiol-terminated oligoethylene glycols and thiol-terminated oligopropylene glycols bound to a  $Au_{10}$  cluster are shown in Figures S10–S13.



**Figure S10.** Linear fit for the superexchange tunneling parameters,  $e_0$  and  $V$ , using DFT orbital energies of oxygen lone pairs of  $Au_{10}S(CH_2CH_2O)_nCH_3$  ( $n = 3-7$ ) in the all-trans conformation.

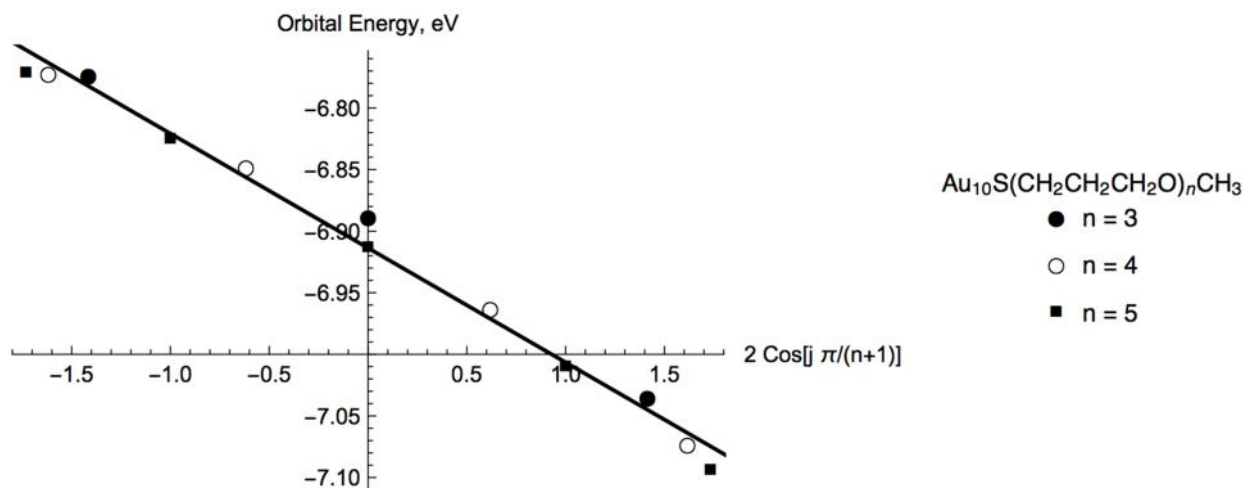




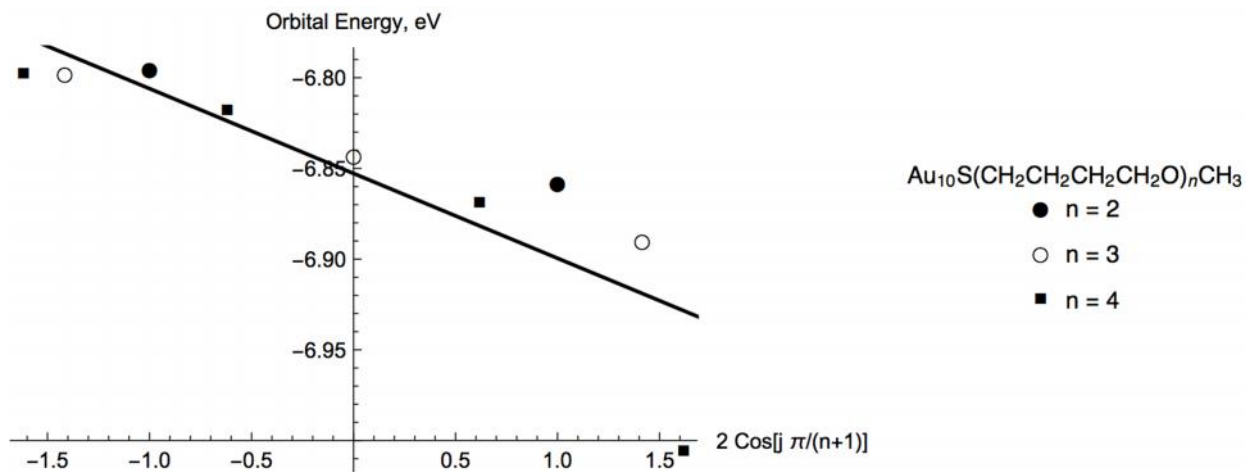
**Figure S11.** Linear fit for the superexchange tunneling parameters,  $\epsilon_0$  and  $V$ , using DFT orbital energies of oxygen lone pairs of  $\text{Au}_{10}\text{S}(\text{CH}_2\text{CH}_2\text{O})_n\text{CH}_3$  ( $n = 3-7$ ) in an all-helical conformation.

We observe good agreement with the linear relationship predicted by the superexchange tunneling model. We obtain  $\epsilon_0 = (-6.99 \pm 0.007)$  eV and  $V = (-0.09 \pm 0.005)$  eV for  $\text{Au}_{10}\text{S}(\text{CH}_2\text{CH}_2\text{O})_n\text{CH}_3$  ( $n = 3-7$ ) in the all-trans conformation and  $\epsilon_0 = (-6.93 \pm 0.008)$  eV and  $V = (-0.15 \pm 0.007)$  eV for  $\text{Au}_{10}\text{S}(\text{CH}_2\text{CH}_2\text{O})_n\text{CH}_3$  ( $n = 3-7$ ) in the all-helical conformation.

The estimated parameters for  $\text{Au}_{10}\text{S}(\text{CH}_2\text{CH}_2\text{CH}_2\text{O})_n\text{CH}_3$  ( $n = 3-5$ ) are  $\epsilon_0 = (-6.91 \pm 0.004)$  eV,  $V = (-0.09 \pm 0.003)$  eV. The gold-bound, thiol-terminated oligo(butane-1,4-diols) show considerably lower nearest-neighbor coupling, however:  $\epsilon_0 = (-6.85 \pm 0.01)$  eV,  $V = (-0.05 \pm 0.01)$  eV.



**Figure S12.** Linear fit for the superexchange tunneling parameters,  $\epsilon_0$  and  $V$ , using DFT orbital energies of oxygen lone pairs of  $\text{SAu}_{10}(\text{CH}_2\text{CH}_2\text{CH}_2\text{O})_n\text{CH}_3$  ( $n = 3-5$ ).



**Figure S13.** Linear fit for the superexchange tunneling parameters,  $\epsilon_0$  and  $V$ , using DFT orbital energies of oxygen lone pairs of  $\text{SAu}_{10}(\text{CH}_2\text{CH}_2\text{CH}_2\text{CH}_2\text{O})_n\text{CH}_3$  ( $n = 1-3$ ).

## 2. Supporting Text

**2.1. Summary of Previous Results on Tunneling Conductivity using EGaIn as the Top Electrode.** Our investigations of charge transport have used a junction comprising EGaIn (a eutectic alloy of gallium and indium) as the top electrode. Three trends summarize the results of our studies using this electrode. i) SAMs composed of insulating (CH<sub>2</sub>) groups (or other aliphatic or simple aromatic groups) present high tunneling barriers, and these high barriers correlate with low rates of charge transport.<sup>14, 27-30</sup> ii) SAMs composed of molecules with a smaller energy gap between the highest occupied molecular orbital (HOMO) and the lowest unoccupied molecular orbital (LUMO) *do* result in increases in the rates of charge transport by tunneling (relative to length-matched *n*-alkanethiolates). The introduction of oligophenyl groups in place of oligomethylene groups, for example, lowers the height of the tunneling barrier, and correlates with an increase in the rates of charge transport.<sup>15, 31</sup> iii) When the structures of the anchoring group and the metal allow the HOMO to delocalize into the R moiety (as with Au/S(C<sub>6</sub>H<sub>4</sub>)<sub>n</sub>H), the resulting changes, and perhaps a decrease in the width of the barrier in this interface, are easily detected by an increase (relative to length-matched *n*-alkyl groups) in rates of charge transport<sup>15</sup>.

**2.2. SAMs Bearing Terminal Groups of Ethylene Glycol for Applications in Protein Resistance.** The characterization of alkanethiolates modified with terminal ethylene glycol units on gold and silver substrates have been described previously, and studied extensively in the context of surfaces that resist adsorption of proteins.<sup>13, 32-36</sup> Alkyl SAMs incorporating terminal units of ethylene glycol (*i.e.*, HS(CH<sub>2</sub>)<sub>11</sub>(OCH<sub>2</sub>CH<sub>2</sub>)<sub>n</sub>OMe) adopt a trans-extended conformation when the number of units is less than six; SAMs having a greater number of units of ethylene glycol formed helices.<sup>12</sup> (The estimate of this length of this transition point from trans-extended to crystalline-helical varies slightly from study to study).<sup>12-13</sup> For SAMs having six or more units of ethylene glycol, the conformation of the chain differs depending on the structure and method of preparation, and ranges from crystalline or helical to amorphous. In applications related to protein resistance, the presence of helical or amorphous ethylene glycol segments aids in the ability of the SAM to resist protein adsorption.<sup>13</sup> Grunze and coworkers have suggested that a prerequisite to protein resistance is the ability of molecules of water to penetrate the SAM.<sup>34</sup>

## References

1. Vanderah, D. J.; Valincius, G.; Meuse, C. W. *Langmuir* **2002**, *18*, 4674-4680.
2. Weiss, E. A.; Kaufman, G. K.; Kriebel, J. K.; Li, Z.; Schalek, R.; Whitesides, G. M. *Langmuir* **2007**, *23*, 9686-9694.
3. Lamont, C. L. A.; Wilkes, J. *Langmuir* **1999**, *15*, 2037-2042.
4. Zharnikov, M.; Frey, S.; Heister, K.; Grunze, M. *Langmuir* **2000**, *16*, 2697-2705.
5. Jiang, L.; Yuan, L.; Cao, L.; Nijhuis, C. A. *J. Am. Chem. Soc.* **2014**, *136*, 1982-1991.
6. Vericat, C.; Vela, M. E.; Corthey, G.; Pensa, E.; Cortes, E.; Fonticelli, M. H.; Ibanez, F.; Benitez, G. E.; Carro, P.; Salvarezza, R. C. *Rsc Adv* **2014**, *4*, 27730-27754.
7. Giron, J. V. M.; Zelaya, E.; Rubert, A.; Benitez, G.; Carro, P.; Salvarezza, R. C.; Vela, M. E. *J. Phys. Chem. C* **2013**, *117*, 24967-24974.
8. Freeman, T. L.; Evans, S. D.; Ulman, A. *Langmuir* **1995**, *11*, 4411-4417.
9. Zhang, Q.; Huang, H. Z.; He, H. X.; Chen, H. F.; Shao, H. B.; Liu, Z. F. *Surf. Sci.* **1999**, *440*, 142-150.
10. Otálvaro, D.; Veening, T.; Brocks, G. *The Journal of Physical Chemistry C* **2012**, *116*, 7826-7837.
11. Vanderah, D. J.; Arsenault, J.; La, H.; Gates, R. S.; Silin, V.; Meuse, C. W.; Valincius, G. *Langmuir* **2003**, *19*, 3752-3756.
12. Valiokas, R.; Svedhem, S.; Svensson, S. C. T.; Liedberg, B. *Langmuir* **1999**, *15*, 3390-3394.
13. Harder, P.; Grunze, M.; Dahint, R.; Whitesides, G. M.; Laibinis, P. E. *J. Phys. Chem. B* **1998**, *102*, 426-436.
14. Bowers, C. M., Liao, K.C., Yoon, H.J., Rappoport, D., Baghbanzadeh, M., Simeone, F.C, Whitesides, G.M. *Nano Lett.* **2014**, *14*, 3521-3526.
15. Bowers, C. M.; Rappoport, D.; Baghbanzadeh, M.; Simeone, F. C.; Liao, K. C.; Semenov, S. N.; Zaba, T.; Cyganik, P.; Aspuru-Guzik, A.; Whitesides, G. M. *J. Phys. Chem. C* **2016**, *120*, 11331-11337.
16. Baghbanzadeh, M.; Bowers, C. M.; Rappoport, D.; Zaba, T.; Gonidec, M.; Al-Sayah, M. H.; Cyganik, P.; Aspuru-Guzik, A.; Whitesides, G. M. *Angew. Chem. Int. Ed.* **2015**, *54*, 14743-14747.
17. Fracasso, D.; Muglali, M. I.; Rohwerder, M.; Terfort, A.; Chiechi, R. C. *J. Phys. Chem. C* **2013**, *117*, 11367-11376.
18. Peng, G.; Strange, M.; Thygesen, K. S.; Mavrikakis, M. *J. Phys. Chem. C* **2009**, *113*, 20967-20973.
19. Quek, S. Y.; Choi, H. J.; Louie, S. G.; Neaton, J. B. *Nano Lett.* **2009**, *9*, 3949-3953.
20. Wold, D. J.; Haag, R.; Rampi, M. A.; Frisbie, C. D. *J. Phys. Chem. B* **2002**, *106*, 2813-2816.
21. Becke, A. D. *J. Chem. Phys.* **1993**, *98*, 5648-5652.
22. Eichkorn, K.; Treutler, O.; Ohm, H.; Haser, M.; Ahlrichs, R. *Chem. Phys. Lett.* **1995**, *242*, 652-660.
23. Weigend, F.; Ahlrichs, R. *Phys. Chem. Chem. Phys.* **2005**, *7*, 3297-3305.
24. Weigend, F. *Phys. Chem. Chem. Phys.* **2006**, *8*, 1057-1065.
25. Andrae, D.; Haussermann, U.; Dolg, M.; Stoll, H.; Preuss, H. *Theor. Chim. Acta* **1990**, *77*, 123-141.

26. Furche, F.; Ahlrichs, R.; Hattig, C.; Klopper, W.; Sierka, M.; Weigend, F. *Wiley Interdiscip. Rev. Comput. Mol. Sci.* **2014**, *4*, 91-100.
27. Simeone, F. C.; Yoon, H. J.; Thuo, M. M.; Barber, J. R.; Smith, B.; Whitesides, G. M. *J. Am. Chem. Soc.* **2013**, 18131-18144.
28. Yoon, H. J.; Bowers, C. M.; Baghbanzadeh, M.; Whitesides, G. M. *J. Am. Chem. Soc.* **2014**, *136*, 16-19.
29. Yoon, H. J.; Shapiro, N. D.; Park, K. M.; Thuo, M. M.; Soh, S.; Whitesides, G. M. *Angew. Chem. Int. Ed.* **2012**, *51*, 4658-4661.
30. Liao, K. C.; Bowers, C. M.; Yoon, H. J.; Whitesides, G. M. *J. Am. Chem. Soc.* **2015**, *137*, 3852-8.
31. Liao, K.-C., Yoon, H.J., Bowers, C.M., Simeone, F.C., Whitesides, G.M. *Angew. Chem. Int. Ed.* **2014**, *53*, 3889–3893.
32. Vanderah, D. J.; Meuse, C. W.; Silin, V.; Plant, A. L. *Langmuir* **1998**, *14*, 6916-6923.
33. Zolk, M.; Eisert, F.; Pipper, J.; Herrwerth, S.; Eck, W.; Buck, M.; Grunze, M. *Langmuir* **2000**, *16*, 5849-5852.
34. Herrwerth, S.; Eck, W.; Reinhardt, S.; Grunze, M. *J. Am. Chem. Soc.* **2003**, *125*, 9359-9366.
35. Schilp, S.; Rosenhahn, A.; Pettitt, M. E.; Bowen, J.; Callow, M. E.; Callow, J. A.; Grunze, M. *Langmuir* **2009**, *25*, 10077-10082.
36. Balamurugan, S.; Ista, L. K.; Yan, J.; Lopez, G. P.; Fick, J.; Himmelhaus, M.; Grunze, M. *J. Am. Chem. Soc.* **2005**, *127*, 14548-14549.